Electronic structure and optical properties of CdMoO$_4$ and CdWO$_4$

Y. Abraham, N. A. W. Holzwarth, and R. T. Williams

Department of Physics, Wake Forest University, Winston-Salem, North Carolina 21709

In previous work, we studied the electronic structure of several molybdate and tungstate crystals having the scheelite structure. The wolframite structure is another common form for molybdate and tungstate materials. In this paper, we compare two chemically similar materials that naturally form in the scheelite and wolframite structures—CdMoO$_4$ and CdWO$_4$, respectively. We compare the electronic structure and approximate optical properties of these materials within the framework of density-functional theory. One major difference between the two materials is in their lower conduction bands, which are dominated by the crystal-field-split d bands of the transition metal. For CdMoO$_4$ the Mo ions have an approximately tetrahedral coordination causing the lower conduction band to be twofold degenerate, while for CdWO$_4$ the W ions have an approximately octahedral coordination causing the lower conduction band to be threefold dengenerate.

I. INTRODUCTION

Cadmium tungstate (CdWO$_4$) and cadmium molybdate (CdMoO$_4$) are interesting materials from several points of view, including their optical, chemical, and structural properties. Optical properties of CdWO$_4$ are of interest because this material has been used as a scintillator for detecting x rays and γ rays in medical applications.[1,2] It has advantages over other scintillator materials due to its relatively large x-ray absorption coefficient and scintillation output, although its relatively long response time is disadvantageous for some applications.

Chemical interest is due to possible catalytic activity of mixed CdMo$_x$W$_{1-x}$O$_4$ crystals, which have been recently studied by Daturi and co-workers.[3,4] These authors found increased catalytic activity for values of x in the range $\frac{1}{8} < x < \frac{1}{4}$.

Structural interest in these materials is due to the fact that CdWO$_4$ crystallizes in wolframite structure while CdMoO$_4$ crystallizes in scheelite structure. These two crystal structures have many examples in ternary molybdate, tungstate, and other ABO$_4$ materials. According to a compilation by Sleight,[5] the wolframite structure is a generally more closely-packed structure, naturally forming in materials with small A^{2+} ions while the scheelite structure naturally forms in materials with larger A^{2+} ions. For example, ZnMoO$_4$ and ZnWO$_4$ have the wolframite structure, while CaMoO$_4$ and CaWO$_4$ have the scheelite structure. In contrast, CdWO4 and CdMoO$_4$ have different crystal structures—the wolframite material (CdWO$_4$) having a slightly larger unit cell volume than that of the scheelite material (CdMoO$_4$). Interestingly, under pressure there seems to be a tendency for the scheelite form of CdMoO$_4$ to transform to the wolframite form[6] and for the wolframite form of CdWO$_4$ to transform to the scheelite form.[7] In their mixed crystal work, Daturi and co-workers[3,4] found that the 50%-50% alloy ($x=\frac{1}{2}$) takes the scheelite structure, while alloys with smaller Mo concentrations have the wolframite form.

In order to build a basis for understanding some of these unusual properties, we have carried out detailed electronic structure calculations for CdWO$_4$ and CdMoO$_4$ within the framework of density-functional theory. In addition to determining the ground-state electronic density and distribution of one-electron eigenstates, we have also estimated the optical dielectric functions and reflectivity for these materials. In Sec. II, the crystal structure is discussed. The calculational methods are presented in Sec. III. Density-functional results are presented in Sec. IV and compared with results for related materials, especially with our recent study of several tungstate and molybdate scheelite materials.[8] The calculated optical properties are presented in Sec. V and discussed with reference to recent reflectivity measurements of Nagirnyi and co-workers.[9,10] A summary and conclusions are presented in Sec. VI.

II. CRYSTAL STRUCTURES

A. CdMoO$_4$—scheelite structure

Cadmium molybdate has the same crystal structure as CaMoO$_4$, CaWO$_4$, PbMoO$_4$, and PbWO$_4$ whose electronic structures were reported in our previous paper.[8] It belongs to the scheelite-type structure with a space group of $I4_1/a \equiv C_{4h}^6$ which is No. 88 in *The International Tables*.[12] This structure has eight symmetry elements and a body-centered orthorhombic primitive cell that includes two formula units of CdMoO$_4$. Each Mo site is surrounded by four equivalent O sites at a bond length of 1.75 Å in approximately tetrahedral symmetry about that site. Each Cd site is surrounded by 8 O sites at bond lengths of 2.40 Å and 2.44 Å in approximately octahedral symmetry. The crystal parameters used in the present paper were taken from the recent measurements of Daturi and co-workers,[4] which are listed in the first column of Table I. For comparison, earlier results are also listed in this table.[11]

B. CdWO$_4$—wolframite structure

Cadmium tungstate has the wolframite-type structure, which is in the monoclinic class, with one axis not orthogonal to the other two.[3,4] This wolframite structure has a space group of $P2/c \equiv C_{2h}^4$ which corresponds to No. 13 in the *International Tables*.[12] In this structure, each W is surrounded by 6 near O sites in approximately octahedral coordination. There are two distinct oxygen atoms present. Type one (O$_1$) forms a bond to one tungsten atom with a very

TABLE I. Compilation of experimental crystal parameters for $CdMoO_4$. Atom positions are specified using the same conventions as in Ref. 8.

		Ref. 4			Ref. 11	
a(Å)		5.156			5.17	
c(Å)		11.196			11.19	
V(Å^3)		148.82			149.55	
	x	y	z	x	y	z
Cd	0.0	0.25	0.625	0.0	0.25	0.625
Mo	0.0	0.25	0.125	0.0	0.25	0.125
O	0.24	0.091	0.0421	0.25	0.11	0.03

short bond length (1.78 Å) and to two cadmium atoms with longer bond lengths (2.41 and 2.27 Å). Type two (O_2) connects to two different W atoms with longer bond lengths (1.91 and 2.15 Å) and to Cd with a bond length of 2.20 Å. The unit cell contains two formula units of $CdWO_4$. Table II lists the measured lattice constants a, b, and c, as well as the nonorthogonal angle β. In this paper, we used the parameters of Daturi and coworkers.[3] Table II also lists other crystallography data for comparison.[4,7,13] The crystal volume of $CdWO_4$ is apparently less than 1% larger than that of $CdMoO_4$, and there is considerable variation in the experimental results.

III. CALCULATIONAL METHODS

The computations were performed using the linearized augmented plane wave method using the WIEN97 code,[14] using the same calculational parameters (muffin-tin radii, reciprocal space truncations, and convergence tolerances) as in our previous calculations on the Ca and Pb molybdates and tungstates in the scheelite structure.[8] Specifically, the muffin-tin radius was chosen to be 1.65 bohr for O, Mo, and W, and 1.90 bohr for Cd. The RKMAX parameter was taken to be 10 and the GMAX parameter was taken to be 14 bohr^{-1}. All relativistic effects including the spin-orbit interaction were taken into account. The exchange-correlation functional was taken within the local-density approximation using the form developed by Perdew and Wang.[15] Brillouin-zone integrations within the self-consistency cycles were performed us-

ing a tetrahedron method[16] using 12 and 16 inequivalent **k** points corresponding to 64 and 48 **k** points throughout the Brillouin zone for the scheelite and wolframite structures, respectively. For calculating the density-of-states and the imaginary part of the dielectric tensor, a denser sampling of the Brillouin zone was needed. For these, we used 35 and 63 inequivalent **k** points corresponding to 216 and 252 **k** points throughout the Brillouin zone for the scheelite and wolframite structures, respectively. The larger number of inequivalent **k** points for the wolframite structure are necessary because of its lower symmetry. We checked the convergence of the **k**-point sampling and found nearly identical results with variations in the number of **k** points of about 15%.

In Sec. IV A, results for the total and partial one-electron density-of-states are presented. In order to avoid the sharp spikes of the tetrahedron method,[16] these are calculated using a Gaussian smearing function[17] of the form:

$$N^x(E) = \sum_{n\mathbf{k}} f^x_{n\mathbf{k}} w_\mathbf{k} \frac{e^{-(E-E_{n\mathbf{k}})^2/\sigma^2}}{\sqrt{\pi}\sigma}. \tag{1}$$

In this equation, $w_\mathbf{k}$ denotes the Brillouin-zone sampling weight factor while $f^x_{n\mathbf{k}}$ denotes the partial density-of-states weight factor. For the total density-of-states N^T, the $f^T_{n\mathbf{k}}$ factor is equal to the degeneracy of the state, while for atomic partial density-of-states the $f^a_{n\mathbf{k}}$ factor is the degeneracy of the state times the charge within the muffin-tin sphere for atom a, averaged over all spheres of that type. The Gaussian

TABLE II. Compilation of experimental crystal parameters for $CdWO_4$. Cd sites are located at the fractional positions $\pm(1/2, y_{Cd}, 3/4)$, W sites are located at the fractional positions $\pm(0, y_W, 1/4)$, and the O_1 and O_2 sites are located at the fractional positions $\pm(x_i, y_i, z_i)$ and $\pm(x_i, -y_i, z_i+1/2)$, where $i=1$ or 2.

		Ref. 3			Ref. 4			Ref. 7			Ref. 13	
a(Å)		5.0289			5.026			5.028			5.02	
b(Å)		5.8596			5.867			5.862			5.85	
c(Å)		5.0715			5.078			5.067			5.07	
β(deg)		91.519			91.47			91.50			91.5	
V(Å^3)		149.39			149.69			149.3			148.84	
	x	y	z	x	y	z	x	y	z	x	y	z
Cd	0.5	0.3027	0.75	0.5	0.3020	0.75	0.5	0.3023	0.75	0.5	0.308	0.75
W	0.0	0.17847	0.25	0.0	0.1784	0.25	0.0	0.1785	0.25	0.0	0.180	0.25
O_1	0.242	0.372	0.384	0.250	0.360	0.393	0.242	0.372	0.383	0.240	0.380	0.380
O_2	0.202	0.096	0.951	0.189	0.099	0.954	0.203	0.098	0.949	0.210	0.10	0.960

smearing parameter was chosen to be $\sigma = 0.05$ eV. In all of the density-of-states plots and also in presentation of the band dispersions (Sec. IV B), the zero of energy is taken at the top of the valence band.

In Sec. V, results for components of the dielectric tensor and for the reflectivity are presented. In fact, calculation of the optical properties of materials is beyond the scope of density-functional theory, which is rigorously a ground-state formalism. However, there has recently been considerable progress toward developing methods for calculating optical properties from first principles, using density-functional results as the starting point.[18,19] As a first step toward investigating the optical properties of CdMoO$_4$ and CdWO$_4$, we have calculated the imaginary part of the dielectric tensor from the LAPW one-electron eigenvalues $E_{n\mathbf{k}}$ and corresponding wave functions $\Psi_{n\mathbf{k}}(\mathbf{r})$ using the approach of Sole and Girlanda[18] and the code developed by Ambrosch-Draxl and Abt.[20] In this approximation, the imaginary part of the dielectric tensor is given by a sum of all transitions between occupied ''initial'' bands $n_i\mathbf{k}$ and unoccupied ''final'' bands $n_f\mathbf{k}$, integrated over the Brillouin zone:

$$\varepsilon_2^{\alpha\beta}(h\nu) = \left(\frac{2\pi\hbar e}{m(h\nu - \Delta)}\right)^2 \sum_{n_i n_f} \int \frac{2 d^3 k}{(2\pi)^3} M_{n_i n_f}^{\alpha\beta}(\mathbf{k})$$
$$\times \delta(E_{n_f\mathbf{k}} - E_{n_i\mathbf{k}} + \Delta - h\nu). \quad (2)$$

This expression depends upon momentum matrix elements in the α and β directions between occupied and unoccupied states according to

$$M_{n_i n_f}^{\alpha\beta}(\mathbf{k}) \equiv \mathrm{Re}[\langle \Psi_{n_i\mathbf{k}} | p_\alpha | \Psi_{n_f\mathbf{k}} \rangle \langle \Psi_{n_f\mathbf{k}} | p_\beta | \Psi_{n_i\mathbf{k}} \rangle]. \quad (3)$$

The so called ''self-energy'' parameter Δ is a type of ''scissors operator,''[21,18,20] which approximates the leading correction to the infamous band-gap underestimation problem of density-functional theory.[22] In the present paper, the value of Δ is estimated from experiment. The Brillouin-zone integration in Eq. (2) is approximated using a modified tetrahedron method.[16,20] The real part of the dielectric tensor is determined by numerically evaluating the Kramers-Kronig relations

$$\varepsilon_1^{\alpha\beta}(h\nu) \approx \delta_{\alpha\beta} + \frac{2}{\pi} \mathcal{P} \int_{\nu_{min}}^{\nu_{max}} \frac{\nu' \varepsilon_2^{\alpha\beta}(h\nu')}{\nu'^2 - \nu^2} d\nu', \quad (4)$$

where $\delta_{\alpha\beta}$ indicates the Kronecker δ function in the directional indices α and β.

Strictly speaking, the equality of Eq. (4) holds only when the integration includes the entire frequency range. However, the integration must exclude part of the low-frequency range because we have only included electronic (no vibrational) contributions to ε_2, and it must exclude part of the high-frequency range because we have only calculated electronic transitions over a 30-eV range. From the form of the Kramers-Kronig transform (4), for $h\nu_{min} \lesssim h\nu \lesssim h\nu_{max}$, one can reasonably argue that the neglected integration in the low-frequency range will contribute a slowly varying negative value, while the neglected integration in the high-frequency range will contribute a slowly varying positive value. These corrections affect the calculation of the reflec-
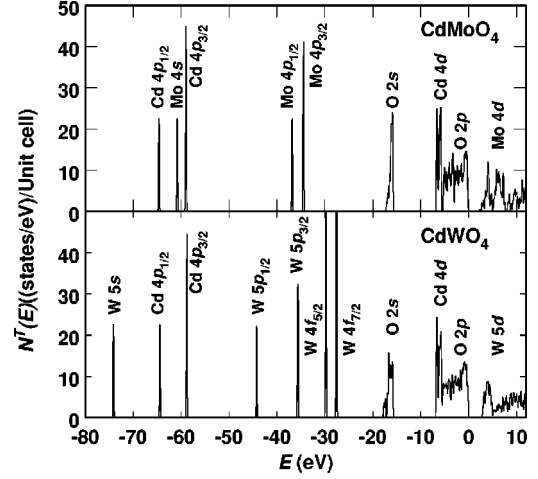

FIG. 1. Total density-of-states of CdMoO$_4$ and CdWO$_4$ including upper core, valence, conduction-band states. The zero of energy is placed at the top of the valence band. Labels represent dominant atomic character of spectral peaks.

tivity and will be discussed further in Sec. V. When the electric-field direction α coincides with an optic axis of the crystal, the corresponding normal incidence reflectivity can then be estimated from the complex components of the dielectric tensor:

$$R_N^\alpha = \left| \frac{(\varepsilon^{\alpha\alpha})^{1/2} - 1}{(\varepsilon^{\alpha\alpha})^{1/2} + 1} \right|^2. \quad (5)$$

This can be conveniently evaluated using the following form:

$$R_N^\alpha = \frac{U^\alpha + 1 - V^\alpha}{U^\alpha + 1 + V^\alpha}, \quad (6)$$

where,

$$U^\alpha \equiv \sqrt{(\varepsilon_1^{\alpha\alpha})^2 + (\varepsilon_2^{\alpha\alpha})^2} \quad \text{and}$$

$$V^\alpha \equiv \sqrt{2\left(\sqrt{(\varepsilon_1^{\alpha\alpha})^2 + (\varepsilon_2^{\alpha\alpha})^2} + \varepsilon_1^{\alpha\alpha}\right)}. \quad (7)$$

In Sec. V we will also discuss the calculation of the reflectivity for other geometries in order to compare with experimental data.

IV. ELECTRONIC STRUCTURE RESULTS

A. Density-of-states

Figure 1 compares the total density-of-states for CaMoO$_4$ and CdWO$_4$ ranging between -80 eV below the top of the valence band to $+12$ eV above the conduction band. The distribution of the Mo and W core states for these materials is very similar to their distribution in the scheelite molybdates and tungstates studied in our earlier work.[8] The Cd $4p$ core states are located close to the Mo $4s$ states in CaMoO$_4$ and 10 eV above the W $5s$ states in CaWO$_4$. For both materials the Cd $4d$ states are concentrated near the bottom of the valence band which, as we will see below, has largely O $2p$ character.
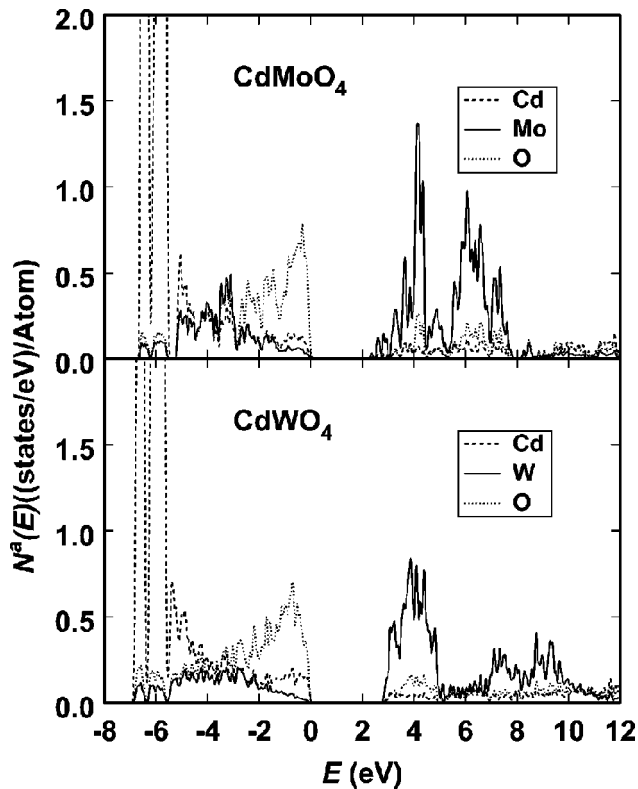
FIG. 2. Partial density-of-states for valence and conduction bands of $CdMoO_4$ and $CdWO_4$, indicating Cd, Mo or W, and O contributions with dashed, solid, and dotted lines, respectively.

Figure 2 shows the partial density-of-states for $CdMoO_4$ and $CdWO_4$ in a 20-eV energy range starting at 8 eV below the top of the valence bands, comparing the spectral contributions from the Cd, W, Mo, and O muffin-tin spheres. Comparing the partial density-of-states plots of these two materials, we see that the main features are similar. One finds the density-of-states features for $CdWO_4$ are generally not as highly peaked as for $CdMoO_4$, due to the lower local symmetry and wider distribution of ligand bond lengths in the wolframite $CdWO_4$ compared with that of the scheelite $CdMoO_4$.

The contributions of the Cd $4d$ states are concentrated in double peaks (due to spin-orbit splitting) of approximate width 1 eV at the bottom of the valence bands of both materials and hybridize to a small extent throughout the valence bands.

The O $2p$ states dominate the upper part of the valence bands and have significant contributions throughout the main portion of the valence bands. From analysis of the electron-density contours, the O $2p$ contributions to the lower and upper valence-band states are primarily σ and π states, respectively, relative to their nearest neighbor Mo or W bonds. For $CdWO_4$, the separation of the σ and π contributions of the O $2p$ states is less well-defined because of the different W-O bond lengths in this structure.

The Mo $4d$ states contribute to a small extent near the bottom of the main valence band in $CdMoO_4$, and dominate the lower conduction bands. As in other scheelite materials, the Mo $4d$ states are split by the tetrahedral crystal field into two groups of states, which will be discussed further below. For $CdWO_4$, the W $5d$ states contribute to a small extent to

the valence bands, with a larger contribution near the bottom of the bands. The dominant contributions of the W $5d$ states occur in the lower portion of the conduction bands where they are split by the approximately octahedral crystal field into two main groups of states.

For the lower portion of the conduction band, contributions associated with the W $5d$ states span more than 7 eV in $CdWO_4$, while those associated with the Mo $4d$ states span less than 6 eV in $CdMoO_4$. For both of these materials the crystal-field splitting of the d states by the approximate octahedral or tetrahedral ligand geometries can be described by twofold degenerate e and threefold degenerate t_2 states. For $CdWO_4$, the lower peak in the conduction-band partial density-of-states is associated with the t_2 states, while the upper peaks are associated with e states, which are actually split into two peaks due to deviations from octahedral symmetry at the W site. For $CdMoO_4$, the lower peak in the conduction-band partial density-of-states is associated with the e states while the upper peak is associated with the t_2 states. Figure 2 shows a very small contribution to the partial density-of-states in the upper conduction-band energy range near 12 eV, although the total density-of-states at these energies is significant. This implies that the states in this energy range are spatially diffuse so that they have very small contributions inside the muffin-tin spheres used for the partial density-of-states analysis.

B. Energy-band dispersions

The Brillouin zones for the scheelite and wolframite structures are shown in Fig. 3. The energy dispersion curves calculated for $CdMoO_4$ and $CdWO_4$ are shown in Fig.4. In both cases the dispersion curves are plotted along three different symmetry directions. Both materials show a group of narrow bands between -6.5 and -5.5 eV corresponding to the Cd $4d$-like states, although other features of the band dispersions are quite different from each other.

For $CdMoO_4$, the minimum band gap of 2.4 eV is located at the Γ point at the center of the Brillouin zone. The valence-band dispersion is similar to that of the scheelite materials $CaMoO_4$ and $CaWO_4$ studied previously.[8] The conduction bands of $CdMoO_4$ are much more dispersive than the corresponding conduction bands of both $CaMoO_4$ and $CaWO_4$. In particular, the Ca materials are characterized by a small band gap between the lower and upper conduction bands that correspond to the crystal-field split states of Mo $4d$ and W $5d$ character, while for $CdMoO_4$ the crystal-field split $4d$ Mo states are not separated by a well-defined band gap.

By contrast, the minimum band gap of 2.9 eV for $CdWO_4$ does not occur at the Γ point, but at Y, which is located at the center of the Brillouin-zone boundary plane perpendicular to the b crystal axis. The valence-band width of 5.3 eV is slightly larger (by 0.3 eV) than the valence band width of $CdMoO_4$. The conduction band of $CdWO_4$ is generally less dispersive than that of $CdMoO_4$.

C. Electron-density maps

In order to further understand the electronic states in greater detail, we have constructed contour plots of the elec-

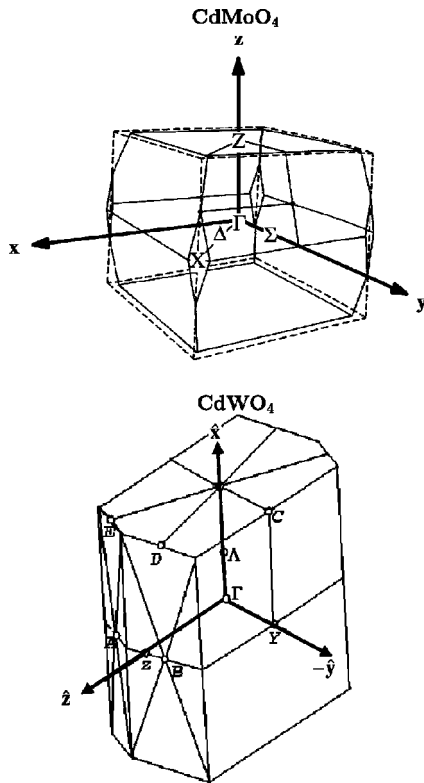FIG. 3. Diagram of the Brillouin zones for CdMoO$_4$ and CdWO$_4$.

tron density associated with selected states. The results for CdMoO$_4$ in the scheelite structure were very similar to those of CaMoO$_4$ presented in our earlier paper[8] and therefore are not presented here.
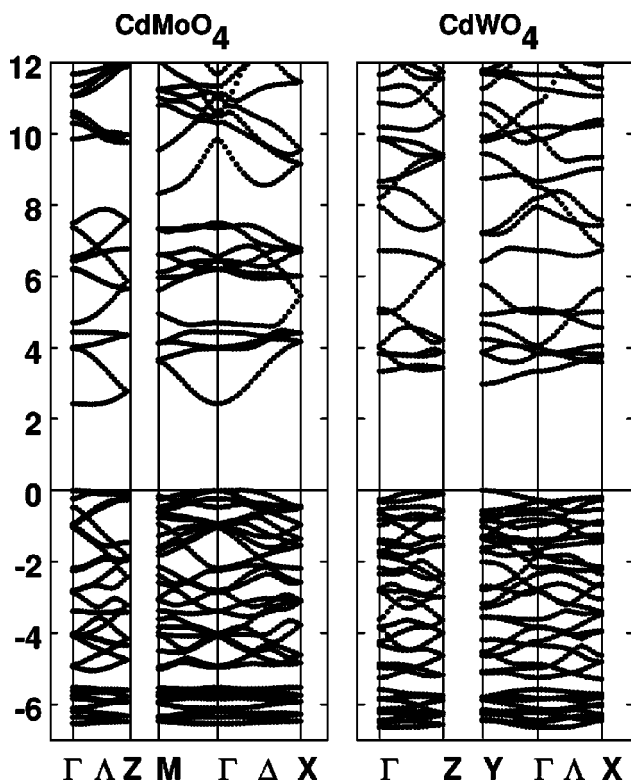

FIG. 4. Energy-band dispersions for CdMoO$_4$ and CdWO$_4$ plotting along Brillouin-zone directions indicated in Fig. 3.
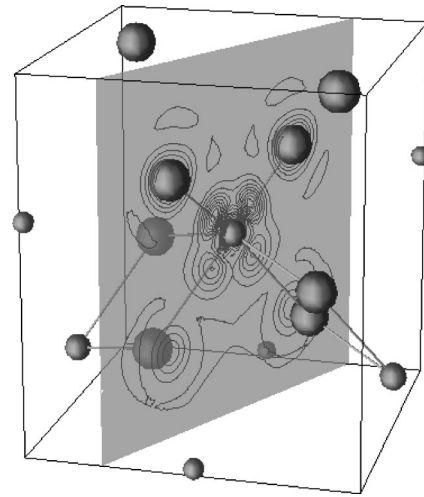

FIG. 5. A perspective drawing of the crystal structure of CdWO$_4$. The spheres represent O, W, and Cd positions using large, medium, small sizes, respectively. The bonds represent the near-neighbor W-O interactions. The shaded plane is drawn to pass through a W atom and its nearest-neighbor O atoms. This is the plane that is used to construct the two-dimensional electron contour plots described below. The contours superimposed on this diagram correspond the upper-conduction-band states presented in Fig. 6(f).

For the electron density of CdWO$_4$, we chose to construct contour plots in a plane that passes through a W site and its nearest-neighbor O sites. Figure 5 shows the drawing of the atoms contained in a unit cell of CdWO$_4$ and of the plane used for plotting the contours. From this figure, we can see the approximate octahedral symmetry about the W site. For perfect octahedral symmetry, the W site would be surrounded by six equidistant O atoms, with four in a plane and two along an axis perpendicular to that plane. In CdWO$_4$, we see that only two O atoms are in the plane, while another two are close to that plane at a larger bond distance. Bonds from the W to the remaining two O atoms have an intermediate length and make an angle with the plane that is only approximately 90°.

Figures 6(a)–6(f) show contour plots of the electron density for various energy ranges of states of CdWO$_4$ in the plane defined in Fig. 5. The contours in Fig. 6(a) correspond to the energy range dominated by the Cd $4d$ states and thus show a very small contribution to the electron density in the W-O plane shown. Plots 6(b) and 6(c) show O $2p\sigma$ orbitals hybridizing with the W $5d$ orbitals, representing the middle portion of the valence band. Plot 6(d) shows the O $2p\pi$ states that comprise the upper portion of the valence band, with very little contribution from the W states.

Plots 6(e) and 6(f) show the electron-density contours for the lower and upper conduction band states, respectively. These plots clearly show the crystal-field split $5d$ states of W. If one compares the shapes of these contours with those of the conduction bands of the scheelite materials plotted in a similar way,[8] one finds that they look very similar. In both structures, the bottom conduction-band state has W $5d$ orbitals that have peak densities in the nonbonding directions and that hybridize with the π states of the nearest-neighbor O atoms. The upper conduction-band state has W $5d$ orbitals that have peak densities along the bond directions, making antibonding hybrid states with the σ states of the nearest-
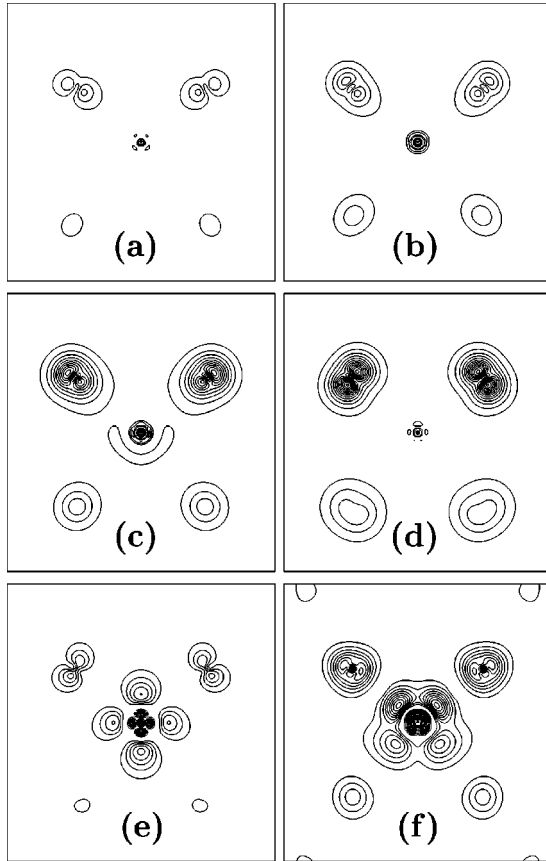
FIG. 6. Contours of electronic charge density for various states of CdWO$_4$ plotted in the plane shown in Fig. 5 with contour levels uniformly spaced at intervals of 0.5 e/Å^3, starting at 0.5 e/Å^3. The one-electron energy ranges for these plots are -7.2 eV to -5.6 eV for (a), and -5.6 eV to -4.0 eV for (b), -4.0 eV to -2.0 eV for (c), -1.8 eV to 0 eV for (d), 2.5 eV to 5.1 eV for (e), and 5.1 eV to 11.9 eV for (f). For plots (e) and (f), the electron density was calculated supposing full occupancy of these unoccupied bands.

neighbor O atoms. There is one important difference between the wolframite and scheelite conduction bands, however. In the wolframite structure, the local symmetry about the W site is approximately octahedral and the lower band is threefold degenerate with t_2 symmetry while the upper band has e symmetry. As shown in Fig. 2, the twofold degenerate e states are split by approximately 2 eV by deviations from octahedral symmetry. In the scheelite structure, the local symmetry about the Mo site is approximately tetrahedral and the lower band is twofold degenerate having e symmetry, while the upper band is threefold degenerate having t_2 symmetry.

V. OPTICAL PROPERTIES

As described in Sec. III, in order to calculate the imaginary part of the dielectric tensor from the density-functional results, it is necessary to estimate a self-energy correction Δ. A rough estimate of Δ is the difference between the experimental band gap and the value determined from our results calculated within the local-density approximation (LDA). Unfortunately, the experimental values of E_{gap} have not been precisely measured. Table III lists the LDA values of E_{gap} compared with several literature results. For CdMoO$_4$, if we take the reference band gap to be 3.8 eV, the average of the two experimental values, the self-energy correction can be taken to be $\Delta = 1.4$ eV. Measurements of the absorption edge in CdWO$_4$ lead to estimates of $E_{gap} = 3.8$ to 4.09 eV.[23,24,26,27] Yochum and Williams[25] have measured the two-photon absorption spectrum of CdWO$_4$ using a 200 fs pulse of 420-nm light and white-light continuum of similar duration. The spectrum covers final-state energies from 4.5 to 5.5 eV. The absorption rises from a finite value at 4.5 eV to a plateau at approximately 4.7 eV. Taking the published linear absorption edge in bulk crystals as a definite lower limit for the band gap and the two-photon absorption plateau at 4.7 eV as a definite upper bound, and finally influenced by measured reflectivity spectra,[9,10] we estimate an interband edge of 4.4 ± 0.3 eV for CdWO$_4$. The value of the self-energy correction, $\Delta = 1.4$ eV, used in the present paper corresponds to the choice of $E_{gap} = 4.3$ eV.

Since CdMoO$_4$ has orthorhombic symmetry, it has two distinct optic axes. The corresponding dielectric tensor components are $\varepsilon^{xx} \equiv \varepsilon^{yy}$, corresponding to the electric field oriented along one of the a axes and ε^{zz}, corresponding to the electric field oriented along the c axis. The calculated values of ε_2^{xx} and ε_2^{zz} and of ε_1^{xx} and ε_1^{zz} are shown in Figs. 7 and 8, respectively. The ε_2 results indicate that the dominant transitions occur within approximately 8 eV above the band gap with two main peaks due to transitions between the O valence band and the crystal-field split Mo $4d$ conduction bands. A small peak near 10 eV is due to transitions from the Cd $4d$ states. The average of the calculated values of ε_1 is close the experimental measurements in the transparent region,[28] although the calculated birefringence is considerably larger than experiment. As discussed in Sec. III there are some systematic errors due to truncation error in the Kramer's-Kronig integral (4) used to calculate $\varepsilon_1^{\alpha\alpha}$. Since $\varepsilon_2^{\alpha\alpha}$ is not zero at ν_{max}, we expect our calculated $\varepsilon_1^{\alpha\alpha}(\nu)$ to be underestimated. The fact that ε_1^{xx} is larger than experiment in the visible range suggests that either the neglected

TABLE III. Estimates of energy-band gaps.

Material	E_{gap} (eV)	Reference
CdMoO$_4$	2.43	LDA (present paper)
	3.96	Excitation energy Ref. 23
	3.72	Absorption edge Ref. 24
CdWO$_4$	2.94	LDA (present paper)
	4.5$\pm$0.2	Two-photon absorption Ref. 25
	3.8	Absorption edge Refs. 26 and 27
	4.09	Absorption edge Ref. 24

FIG. 7. Calculated values of ε_2^{xx} (solid line) and ε_2^{zz} (dotted line) for CdMoO$_4$.
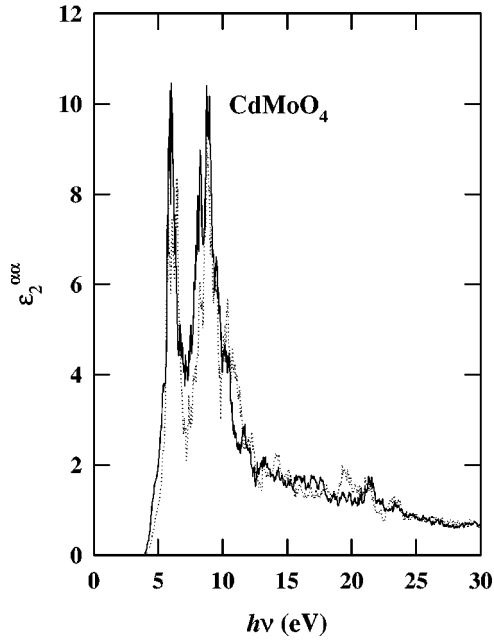
FIG. 9. Calculated values of normal incidence R_N^x (solid line) and R_N^z (dotted line) for CdMoO$_4$.

vibrational contributions of ε_2^{xx} in the Kramer's-Kronig integral are appreciable, or that our calculations generally overestimate the value of ε_2^{xx}.

Using the calculated values of the dielectric tensor components shown for CaMoO$_4$ in Figs. 7 and 8 and Eq. (5), results for the normal-incidence reflectivity are shown in Fig. 9. The calculated reflectivity spectrum shows two main peaks, similar to the spectral form of ε_2. Unfortunately, we do not know of any reflectivity data available for comparison.

Although the crystallographic b and c axes of CdWO$_4$ are mutually orthogonal, the a axis makes an angle of 91.519°
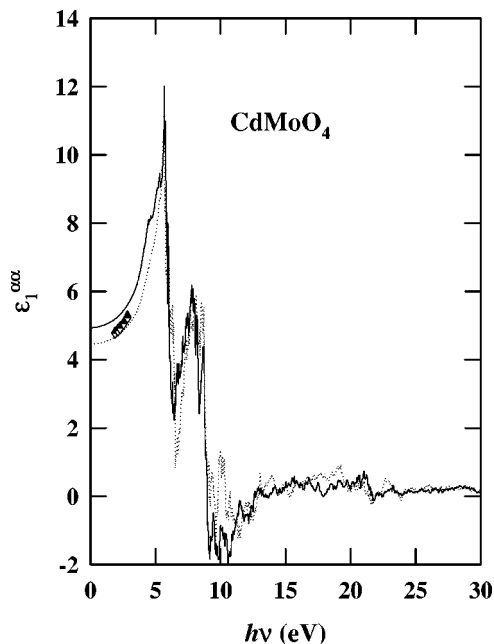

FIG. 8. Calculated values of ε_1^{xx} (solid line) and ε_1^{zz} (dotted line) for CdMoO$_4$. Experimental values from Ref. 28 are plotted with filled and open triangles corresponding to ε_1^{xx} and ε_1^{zz}, respectively.
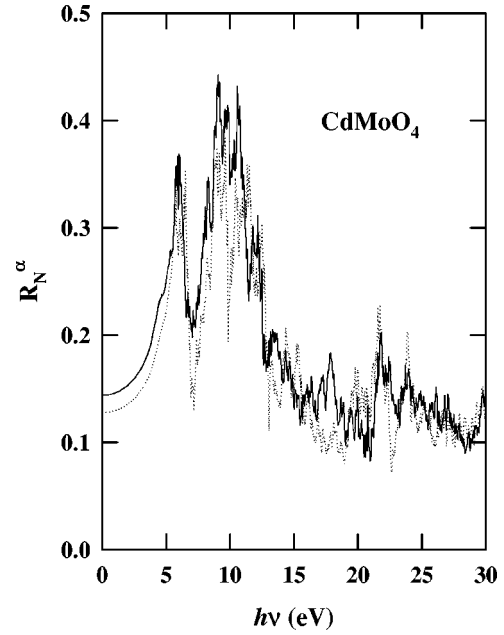
with respect to the c axis in the a-c plane. The principal axis system of the dielectric tensor has been determined experimentally in the transparency region. This axis system includes the crystallographic b axis and two perpendicular axes in the a-c plane. One of those axes is oriented at an angle of 13.5° (Ref. 29) or 16° (Ref. 30) relative to the crystallographic c axis at $\lambda = 633$ nm, and does not rotate appreciably within the transparency region. However, throughout the 30-eV range addressed in the present paper, the principal axes of the dielectric tensor could vary considerably. To facilitate comparisons between theory and experiment referenced approximately to the crystallographic axes, we have adopted a fixed orthogonal coordinate system with the y axis along the crystallographic b axis and the z axis along the crystallographic c axis. The x axis then lies in the $a-c$ plane and makes an angle of 1.519° with the crystallographic a axis. The dielectric tensor expressed in this coordinate system thus has four nontrivial components: $\varepsilon^{xx}, \varepsilon^{yy}, \varepsilon^{zz}$ and $\varepsilon^{xz} \equiv \varepsilon^{zx}$. The remaining elements are zero. These are shown in Figs. 10 and 11 for the imaginary and real parts, respectively. The $\varepsilon_2^{\alpha\alpha}$ spectra for CdWO$_4$ are similar to those of CdMoO$_4$, although the upper-energy peak is smaller and broader than the lower-energy peak. The off-diagonal component ε_2^{xz} is much smaller than the diagonal components. The real parts of the dielectric tensor presented in Fig. 11 are compared with experimental points[29,30] in the transparent region. As for CdMoO$_4$, we find that the average calculated real part of the dielectric tensor is close to the experimental average in the transparent range, although the dispersion and birefringence differ. In addition, one of the principal axes of the dielectric tensor calculated in our results makes a much smaller angle with the z axis than 13.5° or 16° measured by experiment.[29,30] This suggests that our calculated diagonal components of $\varepsilon_1^{\alpha\alpha}$ are comparable or larger than experiment while the calculated off-diagonal ε_1^{xz} is smaller than experiment in the visible spectral region. These discrepancies are partly due to the truncation error in the Kramer's-Kronig
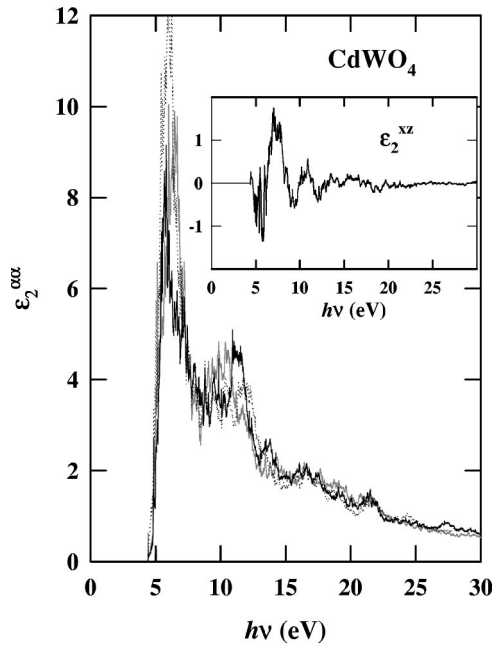
FIG. 10. Calculated values of ε_2^{yy} (solid-black line), ε_2^{zz} (dotted line), and ε_2^{xx} (gray line) for CdWO$_4$. Inset shows off-diagonal element ε_2^{xz}.

transform discussed above and in Sec. III.

Normal-incidence reflectivity, calculated with the electric field oriented along the y axis can be calculated from Eq. (5), while other orientations are more complicated. Since the magnitude of the off-diagonal matrix element ε^{xz} is generally less than 10% of that of the corresponding diagonal components, it is also reasonable to use Eq. (5) to approximate the normal-incidence reflectivity for the electric field oriented along the x and z axes. Figure 12 shows the normal-
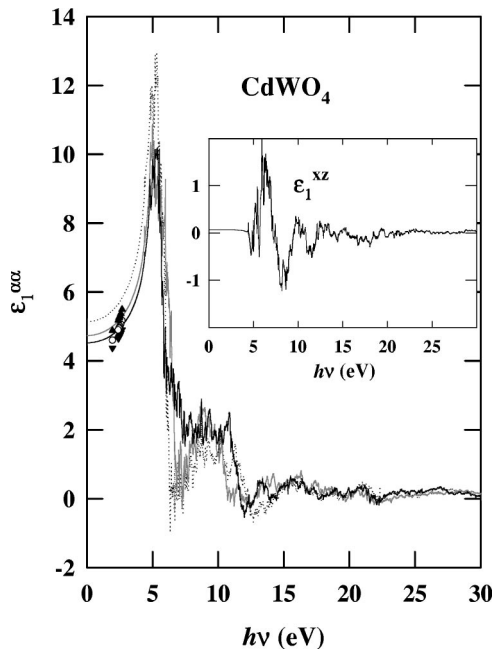

FIG. 11. Calculated values of ε_1^{yy} (solid black line), ε_1^{zz} (dotted line), and ε_1^{xx} (grey line) for CdWO$_4$. Experimental values from Ref. 29 are plotted with filled triangles and open circles corresponding to the three eigenvalues of $\varepsilon_1^{\alpha\beta}$ in the transparent region. Inset shows off-diagonal element ε_1^{xz}.
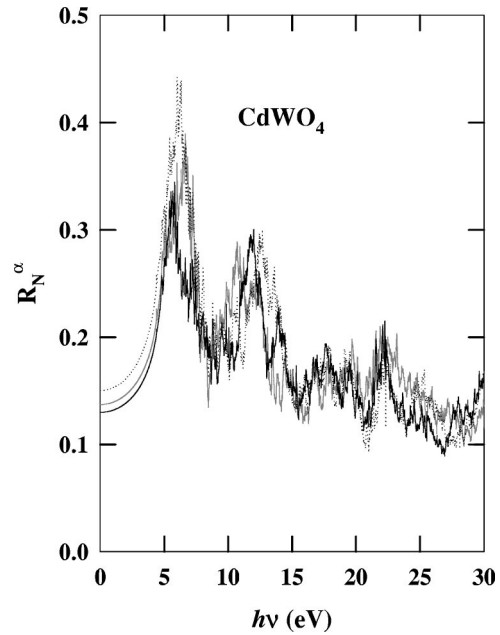

FIG. 12. Values of normal incidence reflectivity for CdWO$_4$; R_N^y (solid-black line), R_N^z (gray line) and R_N^x (dotted line), calculated from Eq. (5), neglecting off-diagonal dielectric contributions.

incidence reflectivity spectra calculated in this way from the uncorrected dielectric tensor components.

Nagirnyi and co-workers[9,10] have measured the reflectivity spectrum of a single-crystal sample of CdWO$_4$, cleaved in the x-z (or a-c) plane. The incident photon beam was oriented with p-polarization at an angle of $\theta = 45°$ relative to the normal direction. Assuming that the off-diagonal dielectric contributions can again be neglected, the corresponding calculated p-polarized reflectivity for an incidence angle of θ and for the electric field in the $y-\alpha$ plane (where α represents either x or z) can be determined from the complex
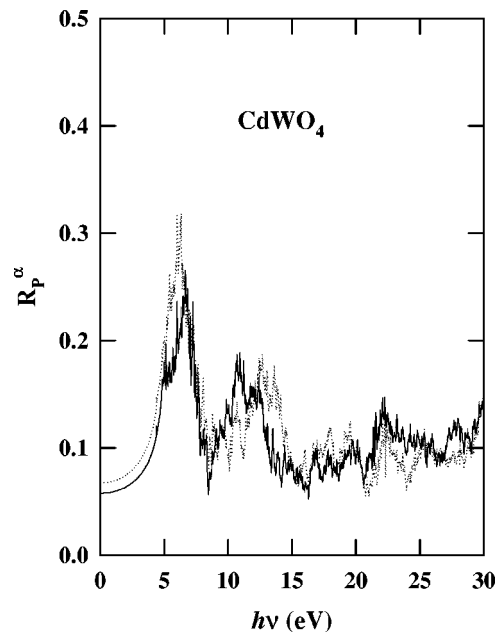

FIG. 13. Values of reflectivity for the z-x (c-a) face of CdWO$_4$ for p-polarization at incidence angle $\theta = 45°$; R_P^z (solid black line) and R_P^x (dotted line), calculated from Eq. (8), neglecting off-diagonal dielectric contributions.

dielectric tensor components according to the equation:

$$R_P^\alpha = \left| \frac{(\varepsilon^{yy} - \sin^2\theta)^{1/2} - (\varepsilon^{yy}\varepsilon^{\alpha\alpha})^{1/2}\cos\theta}{(\varepsilon^{yy} - \sin^2\theta)^{1/2} + (\varepsilon^{yy}\varepsilon^{\alpha\alpha})^{1/2}\cos\theta} \right|^2 . \qquad (8)$$

Results for $\theta = 45°$ are plotted in Fig. 13. The shape of the p-polarized reflectivity spectrum is similar to that at normal incidence, although its magnitude is reduced. Recent preliminary reflectivity measurements of Nagirnyi and co-workers[9,10] demonstrate that the spectra change with crystal orientation. Their data show a two-peak structure below 12 eV, which is qualitatively similar to the results shown in Fig. 13, although features in the spectra at higher energy differ from our calculations. Detailed comparisons will be done in the future.

VI. SUMMARY AND CONCLUSIONS

We have carried out detailed electronic structure calculations for $CdMoO_4$ and $CdWO_4$. The electronic structure of $CdMoO_4$ is similar to that of other scheelite materials, especially to that of $CaMoO_4$. Differences are due to the fact that the $CdMoO_4$ crystal is more compact than other scheelite materials, resulting in larger band widths. In addition, the Cd ions introduce a narrow band of $3d$ character at the bottom of the valence band.

Despite the fact that $CdWO_4$ has the lower-symmetry wolframite structure, there are more similarities than differences of its electronic structure compared with that of $CdMoO_4$. In both materials, the lower-conduction bands are controlled by the crystal-field-split d bands of the transition metal. In the case of $CdMoO_4$, the Mo ions have an approximately tetrahedral environment that causes the lowest-conduction band to be composed of doubly degenerate $4d$-e states. In the case of $CdWO_4$, the W ions have an approximately octahedral environment, which caused the lowest-conduction band to be composed of triply degenerate $5d$-t_2 states. The optical spectra of the two materials are effected by these differences. The calculated imaginary components of the dielectric tensor for $CdMoO_4$ show two peaks of similar strength, while those for $CdWO_4$ show a larger peak near threshold and a smaller peak at higher energy. Detailed comparison of the present results with experiment will be possible as soon as single-crystal optical measurements are completed.[10]

[1] M. Ishii and M. Kobayashi, Prog. Cryst. Growth Charact. **23**, 245 (1991).

[2] S. Chernov, R. Deych, L. Grigorjeva, and D. Millers, Mater. Sci. Forum **239-241**, 299 (1997).

[3] M. Daturi, M. M. Borel, A. Leclaire, L. Savary, G. Costentin, J. C. Lavalley, and B. Raveau, J. Chim. Phys. **93**, 2043 (1996).

[4] M. Daturi, G. Basca, M. M. Borel, A. Leclaire, and P. Paiggio, J. Phys. Chem. B **101**, 4358 (1997).

[5] A. W. Sleight, Acta Crystallogr., Sect. B: Struct. Crystallogr. Cryst. Chem. **B28**, 2899 (1972).

[6] S. R. Shieh, L. C. Ming, and A. Jayaraman, J. Phys. Chem. Solids **57**, 205 (1996).

[7] J. Macavei and H. Schulz, Z. Kristallogr. **207**, 193 (1993).

[8] Y. Zhang, N. A. W. Holzwarth, and R. T. Williams, Phys. Rev. B **57**, 12 738 (1998).

[9] V. Nagirnyi, E. Feldbach, L. J'ónsson, M. Kirm, A. Kotlov, A. Luchchik, L. L. Nagornaya, V. D. Ryzhikov, G. Svensson, I. A. Tupitsina, and M. Åsberg-Dahlborg, in *Tungstate Crystals: Proceedings of the International Workshop on Tungstate Crystals, Rome, October 12-14, 1998*, edited by S. Baccaro, B. Borgia, I. Dafinei, and E. Longo (Università degli Studi *La Sapienza*, Rome, 1999), pp. 155–159.

[10] V. Nagirnyi, 1999 (private communication).

[11] A. V. Chichagov, L. N. Dem'yanets, V. V. Ilyukhin, and N. V. Belov, Kristallografiya **11**, 686 (1966) [Sov. Phys. Crystallogr. **11**, 588 (1966)].

[12] *International Tables for Crystallography*, Vol. A, edited by T. Hahn (D. Reidel, Boston, 1987).

[13] A. P. Chichagov, V. V. Ilyukhin, and N. V. Belov, Dokl. Akad. Nauk (SSSR), **166**, 87 (1966) [Sov. Phys. Dokl. **11**, 11 (1966)].

[14] P. Blaha, K. Schwarz, and J. Luitz (1997), WIEN97, Vienna University of Technology. (Improved and updated Unix version of the original copyrighted WIEN code, which was published by P. Blaha, K. Schwarz, P. Sorantin, and S. B. Trickey, Comput. Phys. Commun. **59**, 399 (1990).

[15] J. P. Perdew and Y. Wang, Phys. Rev. B **45**, 13 244 (1992).

[16] P. E. Blöchl, O. Jepsen, and O. K. Andersen, Phys. Rev. B **49**, 16 223 (1994).

[17] C. L. Fu and K. M. Ho, Phys. Rev. B **28**, 5480 (1983).

[18] R. D. Sole and R. Girlanda, Phys. Rev. B **48**, 11 789 (1994).

[19] M. Rohlfing and S. G. Louie, Phys. Rev. Lett. **81**, 2312 (1998).

[20] C. Ambrosch-Draxl and R. Abt, Synth. Met. **85**, 1099 (1997).

[21] Z. H. Levine and D. C. Allan, Phys. Rev. Lett. **63**, 1719 (1989).

[22] R. W. Godby, M. Schlüter, and L. J. Sham, Phys. Rev. B **37**, 10 159 (1988).

[23] H. J. Zhang, P. Boutinaud, A. Garcia, J. P. Charminade, and C. Fouassier, Solid State Commun. **85**, 1031 (1993).

[24] F. A. Kröger, *Some Aspects of the Luminescence of Solids* (Elsevier, New York, 1948).

[25] H. Yochum and R. T. Williams, 1999 (private communication); based on two-photon absorption spectral measurements for $CdWO_4$.

[26] K. Tanaka, T. Miyajima, N. Shirai, Q. Zhuang, and R. Nakata, J. Appl. Phys. **77**, 6581 (1995).

[27] R. H. Gillette, Rev. Sci. Instrum. **21**, 294 (1950).

[28] G. F. Bakhshieva and A. M. Morozov, Opt. Mekh. Prom. **44**, 31 (1977) [Sov. J. Opt. Technol. **44**, 542 (1977)].

[29] H. Lotem and Z. Burshtein, Opt. Lett. **12**, 561 (1987).

[30] Z. Burshtein, S. Morgan, D. O. Henderson, and E. Silberman, J. Phys. Chem. Solids **49**, 1295 (1988).